Connection of a Topological Surface State with the Bulk Continuum in $Sb_2Te_3(0001)$

Christoph Seibel,[1] Hendrik Bentmann,[1,*] Jürgen Braun,[2] Jan Minár,[2,3] Henriette Maaß,[1] Kazuyuki Sakamoto,[4] Masashi Arita,[5] Kenya Shimada,[5] Hubert Ebert,[2] and Friedrich Reinert[1]

[1]*Experimentelle Physik VII and Röntgen Research Center for Complex Materials (RCCM), Universität Würzburg, Am Hubland, D-97074 Würzburg, Germany*

[2]*Department Chemie, Physikalische Chemie, Universität München, Butenandtstrasse 5-13, D-81377 München, Germany*

[3]*New Technologies—Research Center, University of West Bohemia, Univerzitni 8, 306 14 Pilsen, Czech Republic*

[4]*Department of Nanomaterials Science, Chiba University, Chiba 263-8522, Japan*

[5]*Hiroshima Synchrotron Radiation Center, Hiroshima University, Kagamiyama 2-313, Higashi-Hiroshima 739-0046, Japan*

(Received 7 July 2014; revised manuscript received 8 December 2014; published 10 February 2015)

The surface state of a $\mathbb{Z}_2$ topological insulator connects with the conduction and valence band continua of the bulk, thereby bridging the band gap of the volume. We investigate this connection of the surface and bulk electronic structure for $Sb_2Te_3(0001)$ by photoemission experiments and calculations. Upon crossing the topmost valence band the topological surface state (TSS) maintains a coherent spectral signature, a two-dimensional character, and a linear dispersion relation. Surface-bulk coupling manifests itself in the spectra through (i) a characteristic kink in the TSS dispersion as it crosses the topmost valence band and (ii) the appearance of hybridization gaps between the TSS and bulk-derived surface resonance states at higher binding energies. The findings provide a natural explanation for the unexpectedly weak surface-bulk mixing indicated by recent transport experiments on Sb_2Te_3.

DOI: 10.1103/PhysRevLett.114.066802 PACS numbers: 73.20.At, 79.60.Bm

The hallmark of a three-dimensional $\mathbb{Z}_2$ topological insulator (TI) is a spin-polarized surface state that bridges the fundamental bulk band gap [1,2]. These topological surface states (TSSs) thereby form a two-dimensional (2D) topological metal on the sample surfaces with properties distinct from conventional 2D electron systems [3]. In combination with ferromagnets or superconductors, TIs represent a promising platform for the realization of novel phenomena, such as Majorana bound states [4] or the quantized topological magnetoelectric effect [5]. Unlike for ordinary semiconductors or insulators, the bulk and surface electronic structures of a TI are fundamentally coupled. This coupling is expressed by the concept of bulk-boundary correspondence [1]; that is, a nontrivial topological invariant of the bulk band structure implies the presence of a TSS at the sample boundaries and vice versa. The existence of a TSS is thus determined by the bulk material properties. This is in sharp contrast to conventional surface states that originate from the changed potential landscape in the near-surface region, such as, e.g., the well-known dangling bond states on semiconductor surfaces [6] or Shockley-type surface states in noble metals [7].

The genuine relation between surface and bulk for a TI poses the question how surface and bulk electronic states interact with each other in this unconventional class of materials [8–10]. In particular, the spin-up and spin-down partners of a TSS necessarily couple independently to the conduction and valence band continua, respectively [1,3,11]. This results in an unusual connection of a single spin-polarized surface state branch with the respective bulk continuum that cannot occur in conventional 2D systems and that lies at the heart of the nontrivial topology in the system [3]. Previous works on metal surfaces revealed subtle effects resulting from surface and bulk state interactions (see, e.g., Refs. [12–14]). While scattering between bulk and surface states in TIs has been observed after optical excitation [15], it remains unclear how hybridization with bulk-derived electronic features modifies the TSS dispersion and character. Notably, a thorough understanding of the surface-bulk coupling is also crucial from a technical perspective because in most known TI materials the Fermi level lies in the bulk continuum due to unintentional doping [16]. In this case the TSS may mix with bulk states and thereby lose its well-defined surface character at the Fermi level, e.g., by forming a surface resonance [17].

In this Letter we investigate the connection of a TSS with the bulk valence band continuum for $Sb_2Te_3(0001)$ using angle-resolved photoelectron spectroscopy (ARPES) experiments and fully relativistic one-step photoemission theory. Sb_2Te_3 belongs to the paradigmatic class of chalcogenide TIs with comparably large bulk gaps allowing, in principle, for room-temperature spintronic applications [18–21]. We find that the TSS exhibits a remarkable robustness upon interference with bulk bands and maintains its surface character up to energies far below the valence band maximum. A finite hybridization at the crossing point between the TSS and the topmost valence band significantly increases the group velocity of the TSS and induces a kink in the otherwise linear dispersion relation. At higher binding energies we observe the

formation of avoided crossings between the TSS and bulk-derived surface resonances. These findings indicate a far more complex connection of topological surface and bulk valence bands than expected from previous works in this material class.

ARPES data were acquired at beam line BL-9A of the Hiroshima synchrotron radiation center (HiSOR) using a hemispherical electron analyzer (Scienta R4000). All measurements were performed under ultrahigh vacuum conditions at pressures below 4×10^{-11} mbar, at sample temperatures below 12 K, and in p-polarized light geometry. Single crystals were cleaved at room temperature by *in situ* exfoliation. The crystallographic orientation of the samples was determined by low-energy electron diffraction (LEED).

The ARPES calculations are based on the fully relativistic version of the one-step model [22,23] in its spin-density matrix formulation [24], which is part of the Munich SPRKKR package [25]. This allows us to consider spin-orbit coupling effects in a natural way. Using the spin-polarized LEED (SPLEED) method [26,27], all multiple-scattering events in the initial and final states are accounted for. Thereby the high-energy final state of the photoelectron is calculated by the best available single-particle approach as a time-reversed SPLEED state [28]. Accordingly, the initial state is represented by the retarded one-electron Green function that is obtained for the same semi-infinite half-space. Furthermore, all matrix-element effects are considered in our analysis. Lifetime effects in the final states are included in a phenomenological way using a parametrized complex inner potential $V_0(E) = V_{0r}(E) + iV_f(E)$, where $V_f = 1.5$ eV induces a finite escape depth of the photoelectron. V_{0r} serves as a reference energy inside the crystal with respect to the vacuum level. To account for impurity scattering, a small constant imaginary value of $V_i = 0.025$ eV is used for the initial state. A realistic description of the surface potential is given through a Rundgren-Malmström barrier [29].

Sb_2Te_3 typically shows a heavy p-type doping with the Fermi level E_F intersecting the bulk valence band [20]. The Dirac point of the TSS on the (0001) surface is therefore located in the unoccupied states and not directly accessible by ARPES. It can be shifted in the vicinity of E_F, however, via surface doping [30] or possibly by a reduced bulk doping [31]. Previous experiments determined the Fermi vector of the lower Dirac cone to roughly 0.05 $Å^{-1}$ [30,32,33]. This agrees with the ARPES data in Fig. 1(a), obtained at a photon energy of $h\nu = 12$ eV. At negative wave vectors we observe the TSS crossing E_F at $k_F = 0.063(6)$ $Å^{-1}$, whereas at positive wave vectors its spectral signature is strongly suppressed by matrix-element effects. The linear dispersion of the TSS is traced down to an energy of about −0.1 eV, where it interferes with the M-shaped bulk-derived valence band feature BVB. Near this crossing point the spectral weight of the band BVB is strongly modified, most likely due to a change of the wave function character. At lower energies a surface state RSS with Rashba-type spin splitting and an additional valence band BVB2 are observed.

Figures 1(b) and 1(c) show ARPES data sets acquired with photon energies of $h\nu = 10$ eV and $h\nu = 8$ eV, respectively. The change of excitation energy suppresses the spectral weight of the band BVB and allows us to examine the TSS in more detail. It is evident, in particular from Fig. 1(c), that the TSS dispersion is only weakly perturbed at the crossing point with the bulk feature BVB. The TSS instead maintains a sharp spectral signature and a linear dispersion down to energies around −0.3 eV.

The photon-energy dependences of the spectra are analyzed in more detail in Fig. 2. The data points in

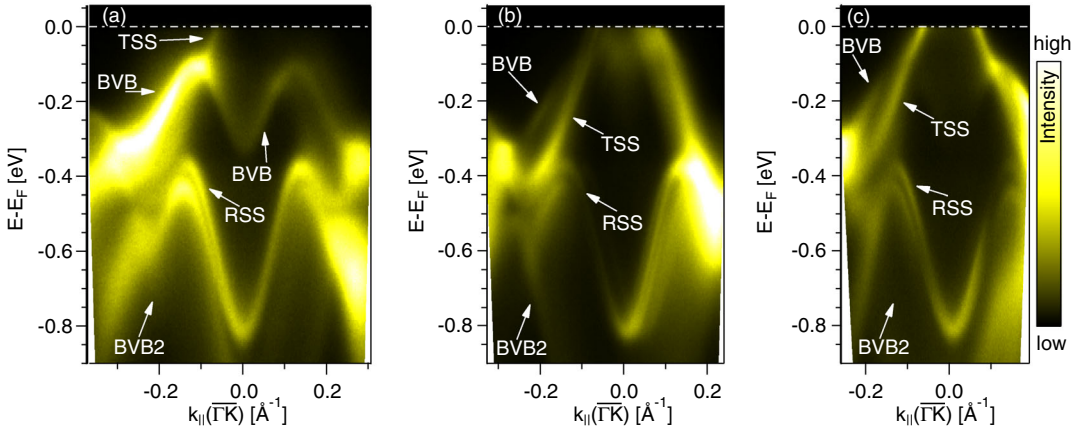

FIG. 1 (color online). ARPES data sets for $Sb_2Te_3(0001)$ along the $\overline{\Gamma K}$ direction measured at photon energies of (a) $h\nu = 12$ eV, (b) $h\nu = 10$ eV, and (c) $h\nu = 8$ eV. The topological surface state (TSS), a surface state with Rashba-type spin splitting (RSS), and two bulk-derived valence band features, BVB and BVB2, are indicated. Photon-energy variation gives rise to strong changes in the relative spectral weights of the individual bands. The TSS maintains a coherent spectral signature and a linear dispersion upon crossing the topmost valence band feature, BVB.

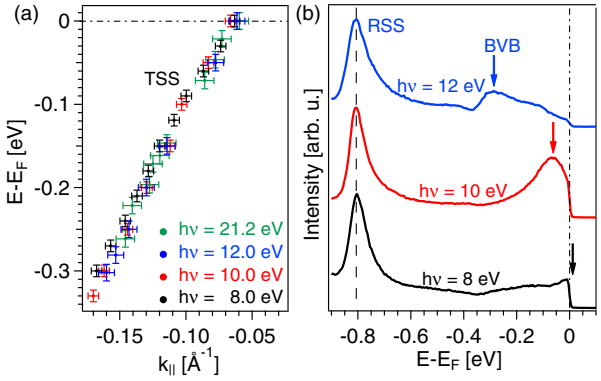

FIG. 2 (color online). Photon-energy dependent analysis of the electronic structure of $Sb_2Te_3(0001)$ near E_F. (a) Peak positions for the TSS obtained from EDC and MDC. The lack of a photon-energy dependence indicates a 2D character of the TSS in the considered energy interval. EDC at the $\bar{\Gamma}$ point are shown in (b). Unlike for the surface state RSS, the energy position of the valence band BVB changes with photon energy indicating its bulk origin near the $\bar{\Gamma}$ point.

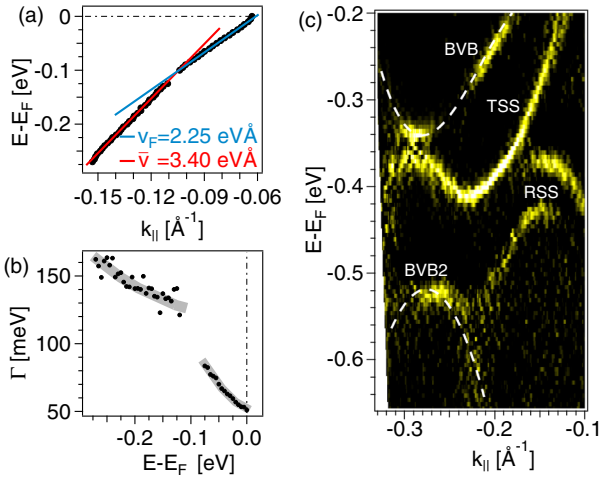

FIG. 3 (color online). Interaction of the TSS with other spectral features. Peak positions and linewidths for the TSS are plotted in (a) and (b), respectively. The data were obtained from MDC of the data set in Fig. 1(c). The group velocity of the TSS abruptly increases when crossing the band BVB at −0.1 eV. Grey bars in (b) serve as guides for the eye. (c) Displays a curvature plot [35] of a section of the data set in Fig. 1(b). It shows a complex band hybridization involving the TSS, the two bulk-derived features, BVB and BVB2, and the two branches of the Rashba-split state RSS.

Fig. 2(a) correspond to intensity maxima obtained from energy and momentum distribution curves (EDC and MDC). Within experimental uncertainty the dispersion of the TSS is independent from the photon energy in the considered energy range. The TSS thus maintains a 2D character even at energies well below the valence maximum.

Figure 2(b) displays EDC at the $\bar{\Gamma}$ point for different photon energies. The energy position of the state RSS remains constant, reflecting its 2D character. On the other hand, variations in the position of the band BVB provide evidence for its bulk origin near the $\bar{\Gamma}$ point. Interestingly, at larger wave vectors beyond the crossing point with the TSS, the photon-energy dependence is reduced and vanishes within experimental uncertainty [see Figs. 1(a)–1(c)]. From bulk band structure calculations, such a decrease in k_z dispersion is not expected [34]. Our data thus indicate a substantial surface character of the feature BVB after crossing the TSS. This is in agreement with our calculations discussed below and suggests assigning this feature to a surface resonance in this $k_\parallel$ regime rather than to a pure bulk state. This scenario complies with the strong $k_\parallel$-dependent intensity changes of the band BVB.

Figures 3(a) and 3(b) show peak positions and linewidths Γ of the TSS, as determined from MDC of the data set in Fig. 1(c). The dispersion of the TSS is nicely described by two linear regimes with different group velocities, as illustrated in Fig. 3(a), giving rise to a hybridization-induced kink at −0.1 eV where the TSS crosses the band BVB. The linewidth increases monotonically with increasing binding energy. At about the energy of the kink, the slope of the increase changes, which points to a correlation between dispersion and linewidth as is well known for quasiparticles, e.g., in the context of electron-phonon interaction. Here, real and imaginary parts of the self-energy, connected via Kramers-Kronig relations, determine the renormalization of the band dispersion and the energy dependent linewidth, respectively. The coupling between TSS and bulk continuum states has previously been explored theoretically within the self-energy picture [8]. In qualitative agreement with our present findings, this coupling was predicted to modify the dispersion and to increase the linewidth of the TSS. We thus propose that hybridization between the TSS and bulk states changes the character of the TSS wave function, namely, its penetration into the bulk and its orbital composition, as a function of energy [8,12], and thereby gives rise to renormalized band dispersion and linewidth evolution near the crossing point with the valence band BVB.

Below approximately −0.3 eV we find deviations from the linearity of the TSS dispersion, as is visible in Fig. 3(c), which shows a curvature plot [35] of a section of Fig. 1(b). The TSS dispersion acquires a considerable bending and even forms a band minimum at −0.41 eV. At about $k_\parallel = -0.28$ Å^{-1} the valence band features, BVB and BVB2, exhibit a band minimum and maximum, respectively, suggesting an avoided crossing between these two features. Bulk band structure calculations indeed predict a hybridization gap of similar size at this $k_\parallel$ position between the two topmost valence bands [31,34]. However, according to our data, the TSS is also involved in the band hybridization which is in line with the assigned surface resonance character of the band BVB in this $k_\parallel$ regime. The strong

bending and the band minimum formation of the TSS dispersion could result from an interaction with the band BVB2. Furthermore, at about $k_{\|} = -0.29$ Å^{-1} one observes a small hybridization gap between the TSS and the feature BVB.

In Fig. 4 we present calculated ARPES data for a photon energy of $h\nu = 10$ eV, which are directly comparable to the measurement in Fig. 1(b). We observe two prominent features in both data sets, labeled with TSS and BVB by comparison with the experiments. Their dispersion is indicated by red and white dashed lines. In reasonable agreement with the experiment, we observe the TSS in the energy range between E_F and about −0.4 eV with almost linear dispersion. Consequently, the TSS intersects the valence band BVB. To support this we first checked the surface character of the TSS using the so-called determinant criterion [36]. In a second step we calculated a series of spectra depending on photon energy. In full agreement with the experimental findings we found a negligible $k_{\perp}$ dispersion. Furthermore, we considered the emission from the band BVB by use of the determinant criterion and found that it acquires a surface resonance character with increasing binding energy. Our calculations also predict an increased group velocity of the TSS after crossing the feature BVB.

To analyze the wave function character of the TSS, we performed a symmetry analysis in suppressing the s- or p-like initial state orbitals in the transition matrix elements [37,38]. The p orbitals are found to play a dominant role over the considered energy range. This implies that interference effects with the valence states do not change the orbital nature of the TSS. Polarization-dependent calculations allow us to quantify the spectral weight of different p orbitals depending on binding energy. This is because the excitation probabilities are strongly

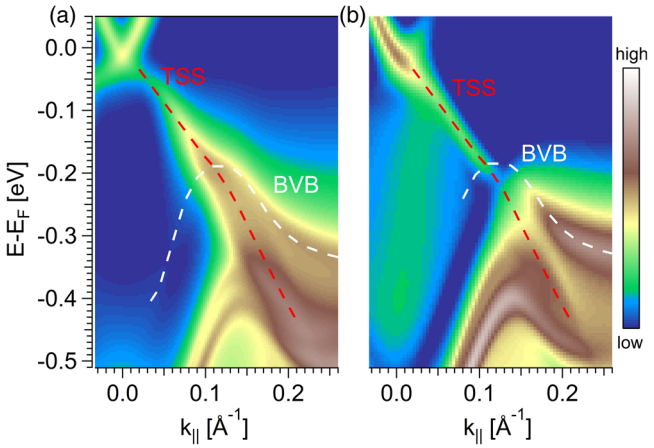

FIG. 4 (color online). Theoretical ARPES data sets for $Sb_2Te_3(0001)$ along $\overline{\Gamma K}$ for a photon energy of 10 eV. The TSS and the bulk feature BVB are indicated. Their dispersions are emphasized by dashed lines serving as guides for the eye. (a) and (b) Data calculated for s- and p-polarized light, respectively.

orbital-dependent quantities and they can differ significantly for the different components of the vector potential in the presence of strong spin-orbit coupling [24]. As an example, we present in Fig. 4 calculated spectra for s-polarized [Fig. 4(a)] and p-polarized [Fig. 4(b)] light. The $p_{x,y}$ orbitals are selectively probed in the first case, whereas p_z orbitals are excited predominantly in the second case. We found that all three types of p orbitals are involved in the emission process, although a redistribution of spectral weight takes place, mainly for binding energies below the crossing point of the TSS and the feature BVB. Again, this is in agreement with the experimental results which provide evidence for hybridization effects between the TSS and the valence band states.

The present findings naturally explain magnetotransport experiments for Sb_2Te_3 that indicated an unexpected robustness of the TSS against mixing with bulk states [39]. Furthermore, our data reveal that the finite coupling between surface and bulk states induces a kink in the linear TSS dispersion. Such hybridization-induced kinks near the connection points of surface and bulk bands could be a quite general effect and might occur similarly in other TI systems. The results also suggest that hybridization between the TSS and bulk states can be "mediated" by bulk-derived surface resonance states. These findings are at variance with band calculations predicting that the TSS wave function will become bulk localized when its dispersion merges with the bulk continuum [40]. They instead favor scenarios where the TSS coexists with bulk and surface resonance states [8]. In previous ARPES reports on related TIs, the TSS dispersion quickly becomes indistinguishable upon interference with the valence band [19,21,41–44]. This is presumably due to a closer proximity of the spectral features in k space that has prevented an experimental resolution so far. Interestingly, our calculations indicate a penetration of the TSS into the bulk continuum and also the appearance of surface resonance states for the conduction band regime in Bi_2Se_3 going along with highly decoupled surface and bulk state dynamics upon optical excitation [45]. The coupling mechanism reported here thus is also likely to occur in similar TI materials and to influence the spin and charge dynamics in these systems.

The synchrotron radiation experiments were performed with the approval of HiSOR (Proposal No. 12-B-35). This work was supported by the Bundesministerium für Bildung und Forschung (BMBF) under Grants No. 05K10WW1/2, No. 05KS1WMB/1, and No. 05K13WMA, the Deutsche Forschunsgsgemeinschaft (DFG) through Grants No. FOR 1162, No. EBE-154/23, No. EBE-154/26, and No. SPP 1666, the Grants-in-Aid for Scientific Research No. (A) 20244045 and No. (B) 25287070, and the CENTEM project, Registration No. CZ.1.05/2.1.00/03.0088, cofunded by the ERDF as part of the Ministry of Education, Youth and Sports OP RDI program. In addition we would like to acknowledge the EU-COST action MP1306 (EUspec).

*Corresponding author.
hendrik.bentmann@physik.uni-wuerzburg.de

[1] M. Z. Hasan and C. L. Kane, Rev. Mod. Phys. **82**, 3045 (2010).
[2] X.-L. Qi and S.-C. Zhang, Rev. Mod. Phys. **83**, 1057 (2011).
[3] L. Fu and C. L. Kane, Phys. Rev. B **76**, 045302 (2007).
[4] L. Fu and C. L. Kane, Phys. Rev. Lett. **100**, 096407 (2008).
[5] X.-L. Qi, T. L. Hughes, and S.-C. Zhang, Phys. Rev. B **78**, 195424 (2008).
[6] R. I. G. Uhrberg, G. V. Hansson, J. M. Nicholls, and S. A. Flodström, Phys. Rev. B **24**, 4684 (1981).
[7] F. Reinert, G. Nicolay, S. Schmidt, D. Ehm, and S. Hüfner, Phys. Rev. B **63**, 115415 (2001).
[8] D. L. Bergman and G. Refael, Phys. Rev. B **82**, 195417 (2010).
[9] Y.-Y. Zhang, M. Shen, X.-T. An, Q.-F. Sun, X.-C. Xie, K. Chang, and S.-S. Li, Phys. Rev. B **90**, 054205 (2014).
[10] Y.-T. Hsu, M. H. Fischer, T. L. Hughes, K. Park, and E.-A. Kim, Phys. Rev. B **89**, 205438 (2014).
[11] M. König, H. Buhmann, L. W. Molenkamp, T. Hughes, C.-X. Liu, X.-L. Qi, and S.-C. Zhang, J. Phys. Soc. Jpn. **77**, 031007 (2008).
[12] A. A. Ünal, C. Tusche, S. Ouazi, S. Wedekind, C.-T. Chiang, A. Winkelmann, D. Sander, J. Henk, and J. Kirschner, Phys. Rev. B **84**, 073107 (2011).
[13] S. N. P. Wissing, C. Eibl, A. Zumbülte, A. B. Schmidt, J. Braun, J. Minár, H. Ebert, and M. Donath, New J. Phys. **15**, 105001 (2013).
[14] H. Bentmann and F. Reinert, New J. Phys. **15**, 115011 (2013).
[15] J. A. Sobota, S. Yang, J. G. Analytis, Y. L. Chen, I. R. Fisher, P. S. Kirchmann, and Z.-X. Shen, Phys. Rev. Lett. **108**, 117403 (2012).
[16] J. G. Analytis, J.-H. Chu, Y. Chen, F. Corredor, R. D. McDonald, Z. X. Shen, and I. R. Fisher, Phys. Rev. B **81**, 205407 (2010).
[17] H. Krakauer, M. Posternak, and A. J. Freeman, Phys. Rev. Lett. **41**, 1072 (1978).
[18] H. Zhang, C.-X. Liu, X.-L. Qi, X. Dai, Z. Fang, and S.-C. Zhang, Nat. Phys. **5**, 438 (2009).
[19] Y. Xia, D. Qian, D. Hsieh, L. Wray, A. Pal, H. Lin, A. Bansil, D. Grauer, Y. S. Hor, R. J. Cava *et al.*, Nat. Phys. **5**, 398 (2009).
[20] D. Hsieh, Y. Xia, D. Qian, L. Wray, F. Meier, J. H. Dil, J. Osterwalder, L. Patthey, A. V. Fedorov, H. Lin *et al.*, Phys. Rev. Lett. **103**, 146401 (2009).
[21] Y. L. Chen, J. G. Analytis, J.-H. Chu, Z. K. Liu, S.-K. Mo, X. L. Qi, H. J. Zhang, D. H. Lu, X. Dai, Z. Fang *et al.*, Science **325**, 178 (2009).
[22] J. F. L. Hopkinson, J. B. Pendry, and D. J. Titterington, Comput. Phys. Commun. **19**, 69 (1980).
[23] J. Braun, Rep. Prog. Phys. **59**, 1267 (1996).
[24] J. Braun, K. Miyamoto, T. Okuda, M. Donath, A. Kimura, H. Ebert, and J. Minár, New J. Phys. **16**, 015005 (2014)
[25] H. Ebert *et al.*, Munich SPRKKR package, version 6.3, http://olymp.cup.uni-muenchen.de/ak/ebert/SPRKKR.
[26] J. B. Pendry, *Low Energy Electron Diffraction* (Academic, London, 1974).
[27] R. Feder, J. Phys. C **14**, 2049 (1981).
[28] A. X. Gray, C. Papp, S. Ueda, B. Balke, Y. Yamashita, L. Plucinski, J. Minár, J. Braun, E. R. Ylvisaker, C. M. Schneider, W. E. Pickett, H. Ebert, K. Kobayashi, and C. S. Fadley, Nat. Mater. **10**, 759 (2011).
[29] G. Malmström and J. Rundgren, Comput. Phys. Commun. **19**, 263 (1980).
[30] C. Seibel, H. Maaß, M. Ohtaka, S. Fiedler, C. Jünger, C.-H. Min, H. Bentmann, K. Sakamoto, and F. Reinert, Phys. Rev. B **86**, 161105 (2012).
[31] C. Pauly, G. Bihlmayer, M. Liebmann, M. Grob, A. Georgi, D. Subramaniam, M. R. Scholz, J. Sánchez-Barriga, A. Varykhalov, S. Blügel *et al.*, Phys. Rev. B **86**, 235106 (2012).
[32] G. Wang, X. Zhu, J. Wen, X. Chen, K. He, L. Wang, X. Ma, Y. Liu, X. Dai, Z. Fang *et al.*, Nano Res. **3**, 874 (2010).
[33] L. Plucinski, A. Herdt, S. Fahrendorf, G. Bihlmayer, G. Mussler, S. Dring, J. Kampmeier, F. Matthes, D. E. Brgler, D. Grtzmacher *et al.*, J. Appl. Phys. **113**, 053706 (2013).
[34] I. Aguilera, C. Friedrich, G. Bihlmayer, and S. Blügel, Phys. Rev. B **88**, 045206 (2013).
[35] P. Zhang, P. Richard, T. Qian, Y.-M. Xu, X. Dai, and H. Ding, Rev. Sci. Instrum. **82**, 043712 (2011).
[36] J. Braun and M. Donath, Europhys. Lett. **59**, 592 (2002).
[37] M. R. Scholz, J. Sánchez-Barriga, J. Braun, D. Marchenko, A. Varykhalov, M. Lindroos, Y. J. Wang, H. Lin, A. Bansil, J. Minár, H. Ebert, A. Volykhov, L. V. Yashina, and O. Rader, Phys. Rev. Lett. **110**, 216801 (2013).
[38] M. Ärrälä, J. Nieminen, J. Braun, H. Ebert, and M. Lindroos, Phys. Rev. B **88**, 195413 (2013).
[39] Y. Takagaki, A. Giussani, K. Perumal, R. Calarco, and K.-J. Friedland, Phys. Rev. B **86**, 125137 (2012).
[40] W. Zhang, R. Yu, H.-J. Zhang, X. Dai, and Z. Fang, New J. Phys. **12**, 065013 (2010).
[41] Y. L. Chen, J.-H. Chu, J. G. Analytis, Z. K. Liu, K. Igarashi, H.-H. Kuo, X. L. Qi, S. K. Mo, R. G. Moore, D. H. Lu *et al.*, Science **329**, 659 (2010).
[42] M. Bianchi, D. Guan, S. Bao, J. Mi, B. B. Iversen, P. D. C. King, and P. Hofmann, Nat. Commun. **1**, 128 (2010).
[43] T. Valla, Z.-H. Pan, D. Gardner, Y. S. Lee, and S. Chu, Phys. Rev. Lett. **108**, 117601 (2012).
[44] C. Chen, S. He, H. Weng, W. Zhang, L. Zhao, H. Liu, X. Jia, D. Mou, S. Liu, J. He *et al.*, Proc. Natl. Acad. Sci. U.S.A. **109**, 3694 (2012).
[45] C. Cacho, A. Crepaldi, M. Battiato, J. Braun, F. Cilento, M. Zacchigna, M. C. Richter, O. Heckmann, E. Springate, Y. Liu *et al.*, Momentum resolved spin dynamics of bulk and surface excited states in the topological insulator Bi_2Se_3, arXiv:1409.5018 [Phys. Rev. Lett. (to be published)].